Journal of Structural Geology, Vol. 9, No. 7, pp. 877 to 891, 1987
Printed in Great Britain

0191-8141/87 $03.00 + 0.00

The last million years of deformation in part of the New Zealand plate-boundary zone

S. H. LAMB and P. VELLA

Research School of Earth Sciences, Victoria University of Wellington, Private Bag, Wellington, New Zealand

(*Received* 15 *September* 1986; *accepted in revised form* 16 *March* 1987)

Abstract—Tectonic deformation of Pleistocene sediments is occurring within the plate-boundary zone in the North Island of New Zealand. Folds, associated with an active fault, are forming mainly by flexural-slip, and contain conformable and unconformable relations which show that the folding started *ca* 1.0 Ma. Simple geometric models of fold growth indicate that the fold structure has shortened at an average rate of 0.76 ± 0.1 mm a^{-1} across 4.5 km, though with an increase in the last 100 Ka of about 1.8 times the average rate, which is entirely compatible with the rate of shortening observed in the last 50 years from retriangulation studies. Areas for 15 km to the southeast of the fold structures show significantly lower horizontal shortening rates. The strain rates across the plate-boundary zone vary both with position and time, with a negative correlation between the uplift pattern and the inferred geological shortening rates. This can be explained by the presence of large semi-rigid blocks within the plate-boundary zone which are back-tilting and overriding weaker more rapidly deforming areas. The available evidence suggests that a large proportion of the deformation is occurring seismically.

INTRODUCTION

AN IMPORTANT problem in structural geology is the way that deformation in continental crust records the relative motions of plates indicated by ocean floor magnetic anomalies. In zones of actively deforming continental crust the seismicity (North 1974, 1977, Anderson 1985) may account for less than 10% of the deformation expected from plate tectonics. Deformation over less than 100 years, derived from geodetic studies, can be shown to be continuous, with total rates that are remarkably similar to the relative plate velocities (Walcott 1984). However, it is not clear what is actually occurring in the crust. Is aseismic deformation the general case, or does the geodetic deformation merely represent the accumulation of elastic strain? Is the long-term deformation continuous in space and time? Is it partitioned? A study of the growth of geological structures in areas where both the relative plate velocities and short-term rates of deformation are known provides an understanding of how deformation is distributed in the crust and at what time scales it is episodic. Dating the deformation shows the time required to produce structural deformation observed in fossil deformation zones.

The relative plate velocities and short-term rates of deformation are known in the New Zealand plate-boundary zone (Walcott 1984). In this paper the last million years of deformation within a small part of the plate-boundary zone is described in detail, and then the deformation across the whole zone is discussed.

Geological setting of the study area

The study area forms part of the emergent actively deforming plate-boundary zone in the southern part of the North Island of New Zealand (Fig. 1). The boundary zone lies between the obliquely converging Australian and Pacific plates, which have a relative velocity in the vicinity of the study area (Pacific relative to Australian plate) of *ca* 50 mm a^{-1} in a direction of 273° [using instantaneous pole and rate from Chase (1978)]. The component of plate motion normal to the boundary zone is *ca* 38 mm a^{-1}, while that parallel to the boundary zone is *ca* 33 mm a^{-1}. Seismic data demonstrate that the region is underlain at a depth of 15–25 km by the gently dipping Pacific plate which is being subducted in the Hikurangi Trench about 100 km to the southeast (Kayal 1984), and hence the plate-boundary zone forms a deformed sedimentary prism (Fig. 2).

The deformed prism consists of a backbone of flysch deposits deformed in a late Palaeozoic–Mesozoic phase of subduction. Mesozoic flysch is unconformably overlain near the study area by conglomerates which pass rapidly into late Tertiary and early Quaternary fine-grained marine sediments deposited in basins related to a renewed phase of subduction. Because of recent uplift these pass up into coarse-grained Pleistocene and younger marginal marine and terrestrial deposits. The stratigraphy, distribution and age of rocks within the study area are summarized in Figs. 3–6 (see also Collen & Vella 1984, Vella & Briggs 1971). These sediments are now deformed in a fold and fault belt oriented approximately parallel to the trench. This forms the emergent part of the plate-boundary zone (total width *ca* 200 km), which contains a zone of strike-slip faults *ca* 45 km wide on the northwest side (Figs. 1 and 2).

FIELD OBSERVATIONS

The strata have a regional dip of *ca* 15°NW containing two slightly oblique zones, one dipping steeply NW and

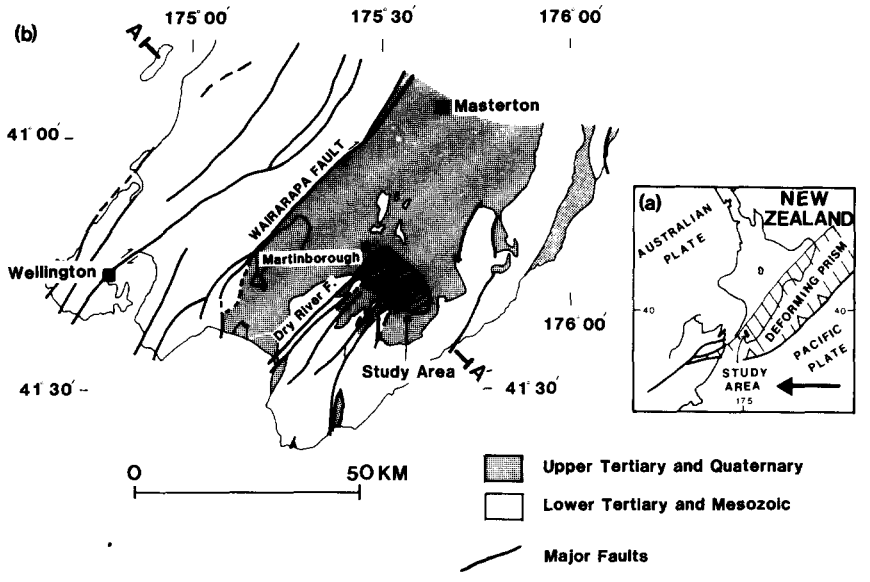

Fig. 1(a). Location map of the study area within the plate-boundary zone in North Island, New Zealand. Crust which is sitting directly on the subducted Pacific plate is shaded; also shown is the velocity vector (50 mm a^{-1}) for the Pacific plate relative to the Australian plate. (b) Simplified geological map of the southern part of North Island, New Zealand (after Kingma 1967), showing the major structural features. The detailed location of the study area is shown as two parts: the cross-hatched area is shown in Fig. 3 and contains the fold structures discussed in the text; the obliquely shaded region contains a uniform gently dipping sequence from the Miocene to Upper Pliocene, and is referred to as the gently dipping regions in the text. Line AA′ marks part of the line of cross-section in Fig. 2, normal to the general structural trend.

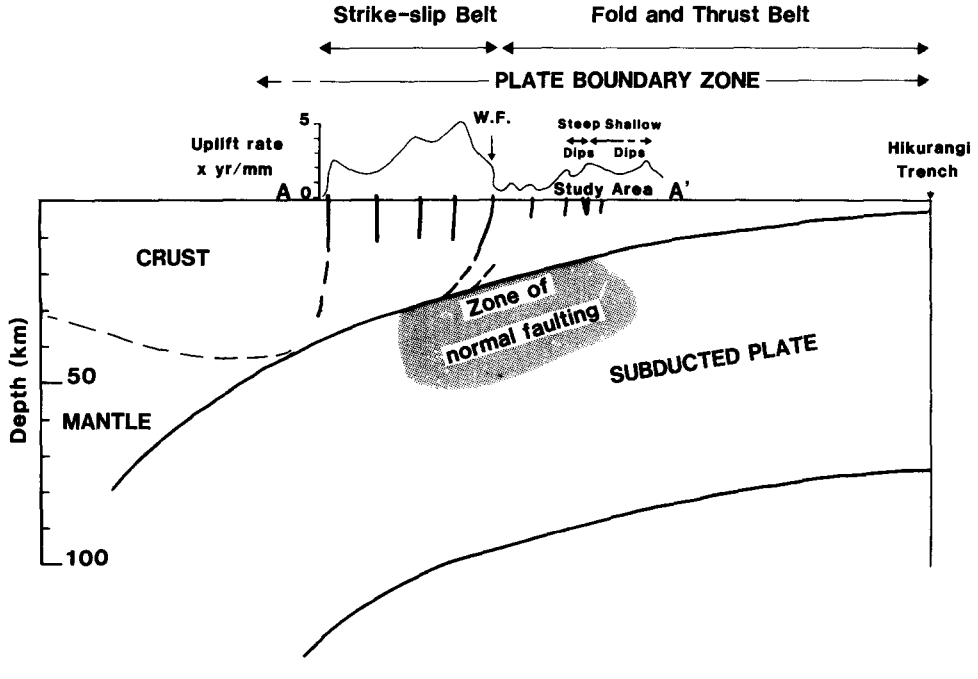

Fig. 2. Cross-section through the plate-boundary zone (see line AA′ in Fig. 1b) roughly normal to the trench and general structural trend, showing the position of the subducted slab. The subducted slab is characterized by seismicity with a dominance of normal fault-plane solutions, in contrast to thrust and strike-slip fault-plane solutions in the overlying plate (after Kayal 1984, Stern *et al.* 1986). The study area is only about 15 km above the top of the Pacific plate. Also shown is the pattern of uplift in the emergent part of the plate-boundary zone, and the position of major faults (heavy lines); the major strike-slip Wairarapa Fault is marked W.F. This fault separates the plate-boundary zone into the strike-slip belt and the fold and thrust belt.

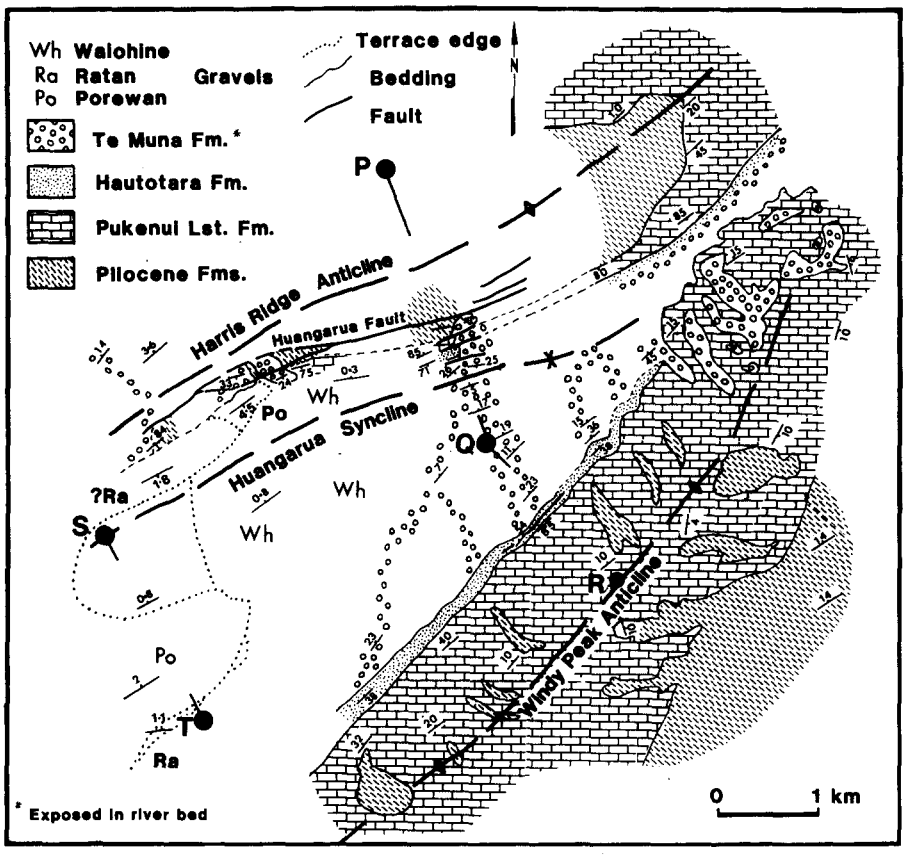

Fig. 3. Detailed geological map of study area. Cross-section along line PQR is shown in Fig. 4. Line ST is discussed in text.

the other dipping steeply SE (Figs. 3 and 4). The steeply-dipping zones define the nearly horizontally plunging asymmetric Harris Ridge Anticline and Huangarua Syncline that form a SE-verging fold pair linked by a faulted steep limb, which at places is overturned (Figs. 4–6). The axial traces of the folds extend for several kilometres as gently sinuous lines within 25° of the regional trend.

On the NW limb of the Huangarua Syncline, gently-dipping gravels of the Te Muna Formation, offset by a series of reverse faults (including the Huangarua Fault), unconformably overly the overturned sequences (Figs. 5 and 6). The late lower Pleistocene Hautotara Formation dips 70°SE and passes conformably into fluvial conglomerates and sandstones of the Te Muna Formation. However about 20 m up the section from the

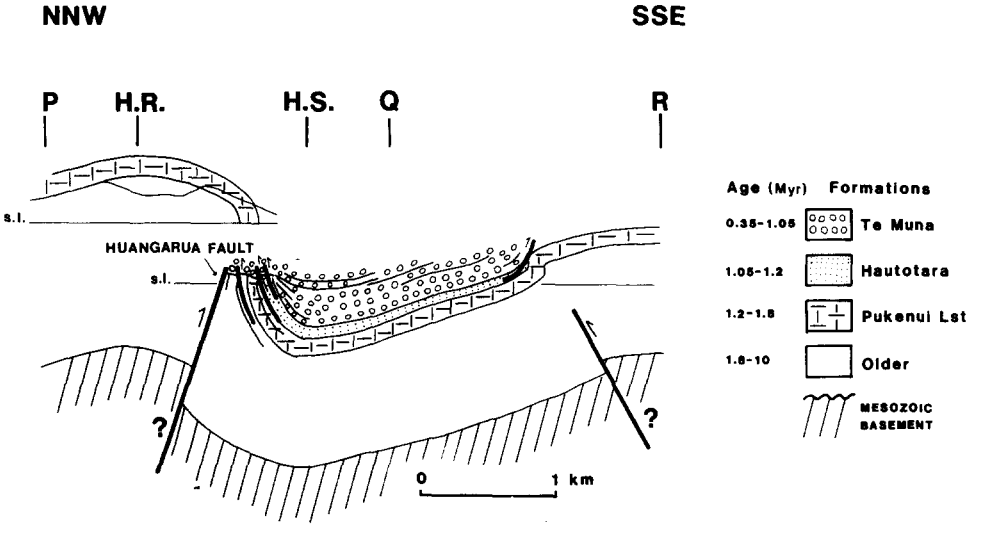

Fig. 4. Vertical cross-section of study area along line PQR in Fig. 3. The crest of the Harris Ridge Anticline is marked H.R.; the trough of the Huangarua Syncline is marked H.S.; R marks the crest of Windy Peak Anticline. The structure of the Harris Ridge Anticline is taken from along strike (different sea level datum) which was not eroded during deposition of the Te Muna Formation. Position of the Mesozoic basement is speculative, although consistent with known stratigraphy. Down-dip extension of the Huangarua Fault and the fault below the Windy Peak Anticline are also speculative.

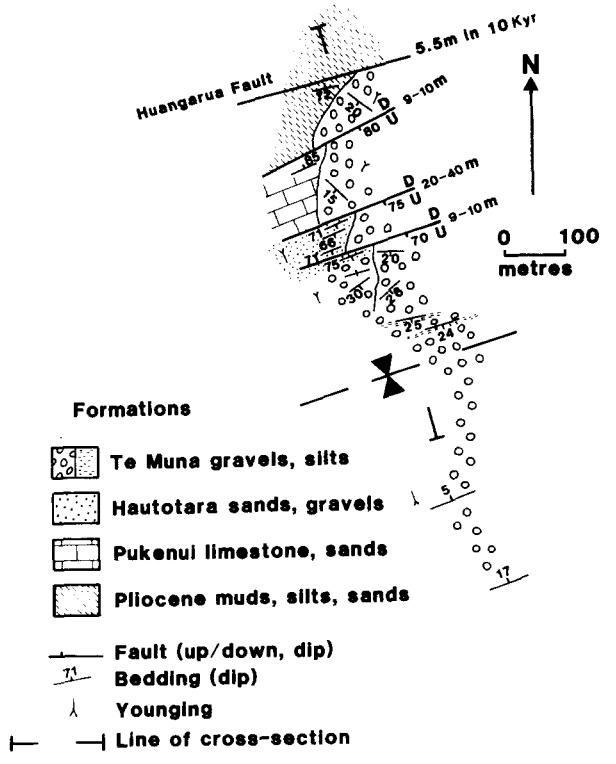

Fig. 5. Detailed geological map of the steep limb of the Huangarua Syncline, outcropping in the Huangarua River. The Huangarua Fault and adjacent flexural-slip faults offset unconformity surface; dip-slip on flexural-slip faults are shown, as well as vertical throw of the Huangarua Fault in the last 10 Ka. The Pukenui Limestone Formation does not actually outcrop in river section, as overlying unconformity surface is below the river level, but is inferred from along strike correlation. Cross-section shown in Fig. 6.

contact, the dip of the conglomerates abruptly fans from 70–80°SE to about 30°SE (Fig. 7). An angular unconformity separates these gravels from those dipping at about 18°SE, which pass laterally into conglomerates which unconformably overly the steeply-dipping sequence (Fig. 7).

The SE limb of the Huangarua Syncline dips gently from 5 to 20°NW. The Windy Park Anticline has a consistent NE trend, slightly oblique to the Huangarua Syncline (*ca* 20°), defining a monoclinal flexure steepening the adjacent limb of the Huangarua Syncline. The Hautotara Formation and Pukenui Limestone Formation are again exposed in the steep limb of the Windy Peak Anticline, passing conformably into the Te Muna Formation. The Te Muna Formation can be traced across the syncline into gravels which unconformably overly the Hautotara Formation on the steep limb of the syncline. For a further 10 km to the southeast of the Windy Peak Anticline, the strata dip 15–20°NW.

Deformation of alluvial terrace surfaces

Younger fluvial gravels, deposited in major phases of alluvial aggradation (Porewan Gravel, *ca* 70 Ka, Fig. 8a&b; Ratan Gravel, *ca* 35 Ka, Fig. 8a) (Milne 1972, Palmer 1982), rest unconformably on the older sequences, but are also folded by the Huangarua Syncline and Harris Ridge Anticline (Table 1, Figs. 9 and 10). These gravels are identified by a distinctive cover of loess laid down during younger alluvial aggradation events. The loess cover forms a mantle to the gravels and does not exceed a few metres in thickness, and so the gradient of the present land surface approximates the tectonic and depositional tilt. For this reason land surfaces are sometimes called by the same name as the gravels immediately below. The gradients of existing braided streams indicate that the depositional tilt of fluvial gravels in the area is not likely to exceed 0.4°. A contour map (Fig. 9) and cross-sections (Fig. 10) clearly show tilts which are consistent with the fold, with contours running subparallel to the Huangarua Syncline axis. Younger Waiohine Gravel (*ca* 10 Ka) has dips between 0.2° and 0.8°N or NW, right across the fold axis

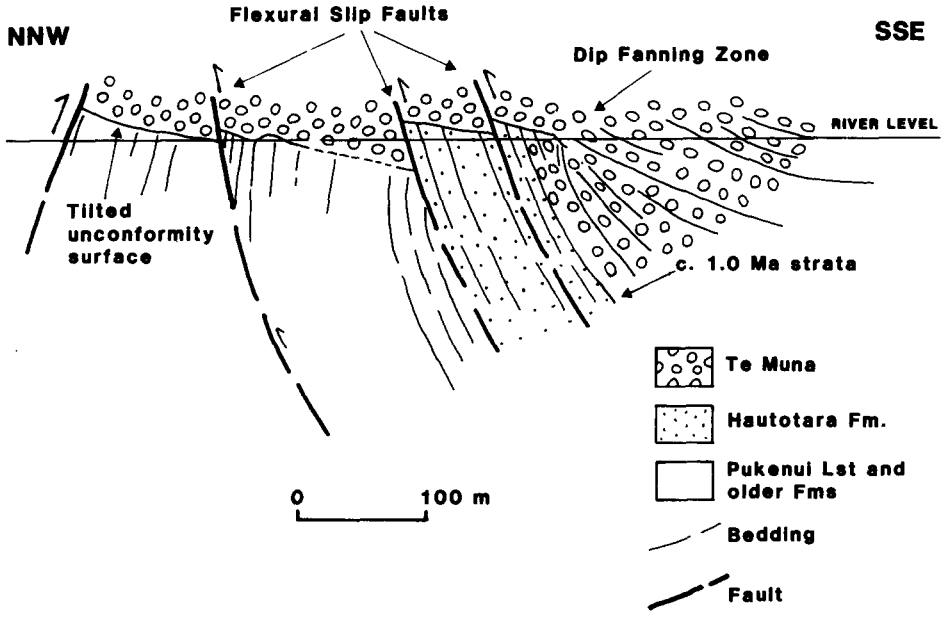

Fig. 6. Cross-section of steep limb of the Huangarua Syncline (see Figs. 4 and 5). Features of cross-section described in text.

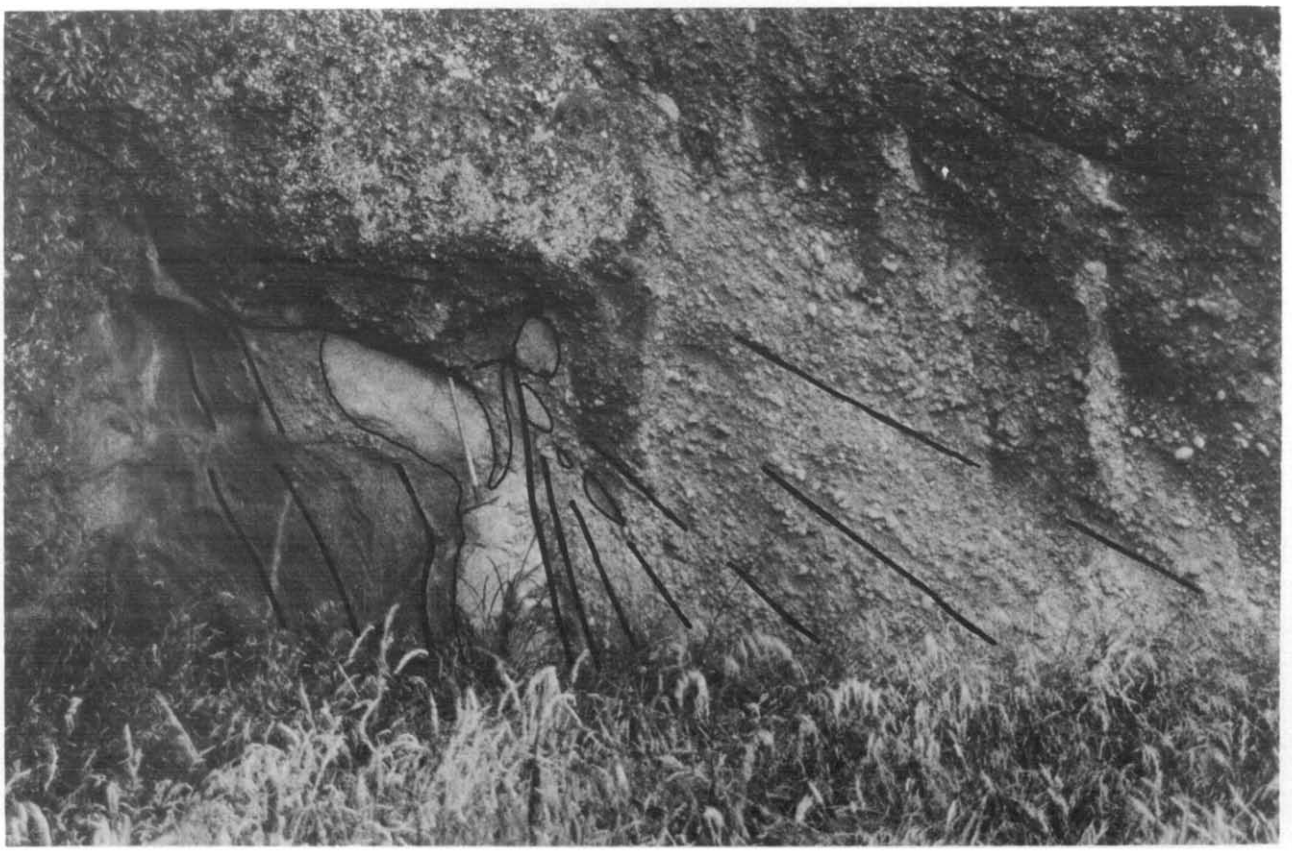

Fig. 7. View, with interpretation, of zone of dip fanning, showing change in dip from subvertical, parallel to sequences below unconformity surface, to gently dipping and parallel to beds above unconformity surface. Pick (centre of photograph) is 1 m long.

Fig. 8(a). View of terraces on the shallow limb of the Huangarua Syncline, dipping towards the core; Po = Porewan surface, Ra = Ratan surface, Wh = Waiohine surface. Terraces here formed in a region of uplift on the fold limb, and hence successive downcutting resulted in younger terraces at lower altitudes. (b) View of remnants of the Porewan Gravel [Porewan surface (Po) arrowed] on the steep limb of the Huangarua Syncline, dipping towards the core at 4–5°. Gravels are overlain by two layers of loess which have partly eroded away in places. Subsequent erosion has resulted in a scarp separating the Porewan surface from that underlain by the Waiohine Gravel (in the foreground).

Table 1. List of tilt data (errors take into account uncertainty in depositional tilt) and rates for various parts of the fold structures and strata of different ages

		(All dips in degrees)				
Age (Ma)	Harris Ridge Anticline NNW dips	Huangarua Syncline SSE	NNW	Windy Peak Anticline NW	NW (Regional)	MATR*
1.8–1.2	5–10	95–105	—	35–100	15–20	8.7–0.27
1.2–1.05	—	70–90	—	35–90		8.6–2.9
1.00	—	70–90	25			7.5–2.5
0.75	—	—	22	10		2.9–1.3
0.5–0.4	—	25–15	5–10			6.3–1.0
0.4–0.3	—	15–10	5?			5.0–1.3
(0.25)	10–14					5.6–4.0
(0.125)	3–4					3.2–2.4
0.07		4.5 ± 1	2 ± 0.4			5.7–2.8
0.035		1.8 ± 0.4?	1.1 ± 0.4			4.6–3.1
0.01		−0.3 ± 0.4†	0.55 ± 0.25			8.0–0.0

* Minimum average tilt rate [tilt (degrees)/stratigraphic age] in units of 10^{-5} degrees a^{-1}.
† Dips NNW.
Ages in brackets uncertain.

up to the scarp of the Huangarua Fault. The small tilt of the surface between the axis of the syncline and the Huangarua Fault is likely to be entirely depositional, and hence the surface here has suffered no tectonic rotation. However the tilt on the SE limb of the syncline (0.8°) is significantly greater than any depositional tilt.

Faulting

The steep limb of the Huangarua Syncline is cut by a series of faults (Figs. 4 and 6) which appear to be

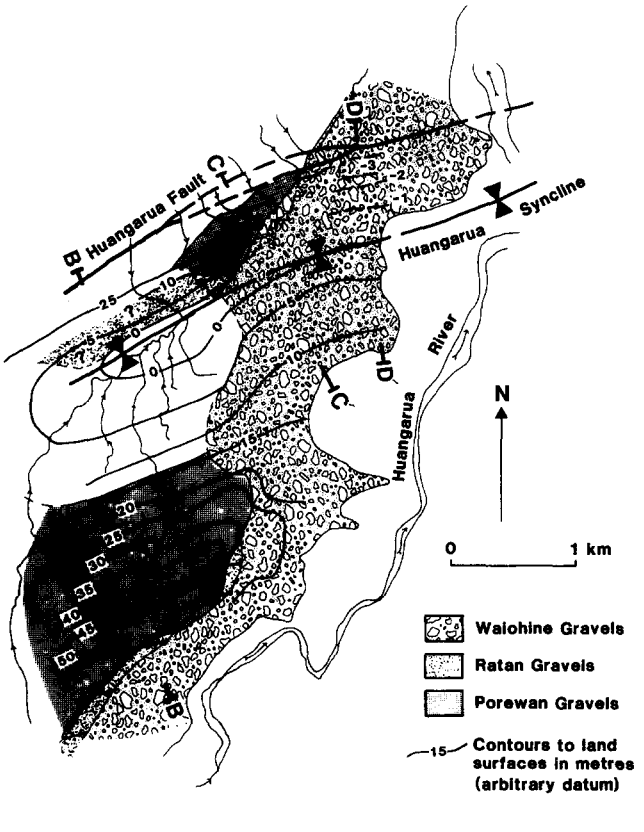

Fig. 9. Contour map of land surfaces overlying younger alluvial gravels. See Fig. 10 for cross-sections.

accommodation structures related to the folding. The active Huangarua Fault has raised the Waiohine surface vertically by up to 6 m on the NW side (in the opposite sense to the adjacent faults). It has not been possible to determine a strike-slip component. The fault in detail has a bifurcating sinuous trace, trending between 060 and 070°, and parallel to the strike of the strata. Its relation to the topography suggests that it dips steeply to the northwest. Cross-sections (Fig. 11) of the Waiohine surface across the fault show a scarp which is abrupt in places, rising 5 m in 30 m horizontally (cross-section ZZ′ in Fig. 11). A distinct bench within the scarp (*ca* 1.5 m below the top of the scarp) may represent the last movement of the fault. The total scarp height may therefore be the result of at least four earthquakes. Along strike (cross-sections YY′ and XX′ in Fig. 11) the scarp passes into a more distributed zone of uplift about 150 m wide, which contains two smaller scarps and an intervening area of significantly tilted surface. Here conglomerates of the Te Muna and younger formations are offset vertically less than 20 m across the fault. To the NW the fault passes into a continuation of the Harris Ridge Anticline, and here no offset can be found in the limestones. All this suggests that the fault in this region is young, perhaps less than a few tens of thousands of years old.

Other reverse faults offsetting the base of the Te Muna Formation are interpreted as flexural-slip faults related to folding. Slickensides indicate slip directions pitching within 10° of the dip direction (i.e. approximately normal to the fold axis). The faults do not appear to have been active in the last 10 Ka as no detectable ground surface offsets can be found where they pass beneath the Waiohine gravels.

The zone of faults is approximately on line with the Dry River Fault (Fig. 1) which offsets Pliocene and older rocks vertically by hundreds of metres, upthrown with the same sense as the Huangarua Fault. The Dry River Fault may represent a deeper structural level to the folds in the study area.

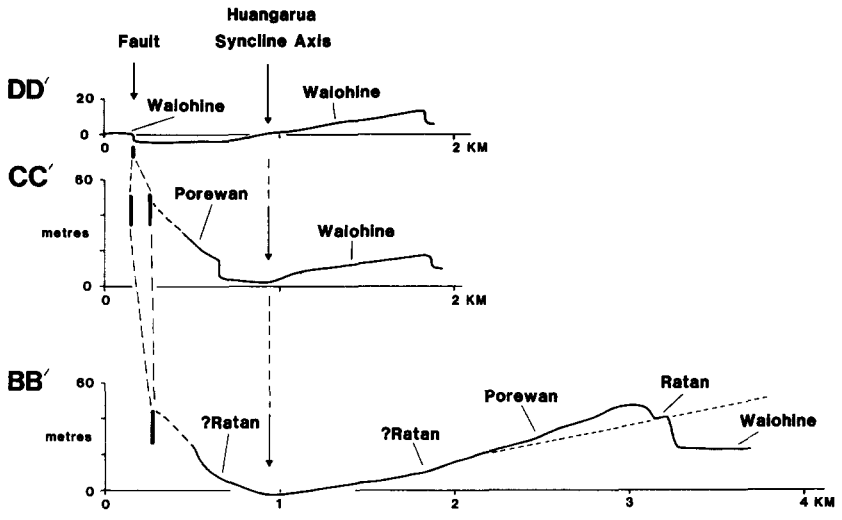

Fig. 10. Topographic cross-sections in the vicinity of the Huangarua Syncline. Line of cross-sections shown in Fig. 9.

Mechanism and age of folding

Sediments within the steep limb of the Huangarua Syncline are internally undeformed. The fold does not contain a cleavage and large truncation angles are preserved in cross-bedded units. Minor faulting is rare, consisting of faults cutting bedding at high angles with displacements of a few centimetres indicating very limited (<5%) extension parallel to the dip of the beds.

The presence of bedding plane dip-slip faults suggests that flexural-slip accommodated along discrete planes has been an important mechanism of folding. If so, the fault displacement should show the expected flexural-slip during the rotation of the unconformity surface at the base of the Te Muna Formation (dipping 15–18° in the plane of the cross-section). The observed down-dip slip on individual faults varies from 9 to possibly 40 m, representing a cumulative slip of 40–60 m across *ca* 300 m of stratigraphy, which is somewhere between 50 and 80% of the expected flexural-slip (approximately θ m of slip per m of stratigraphic thickness for a rotation of θ radians). The flexural-slip faults appear to cut across overturned beds, rather than become overturned themselves (Fig. 6).

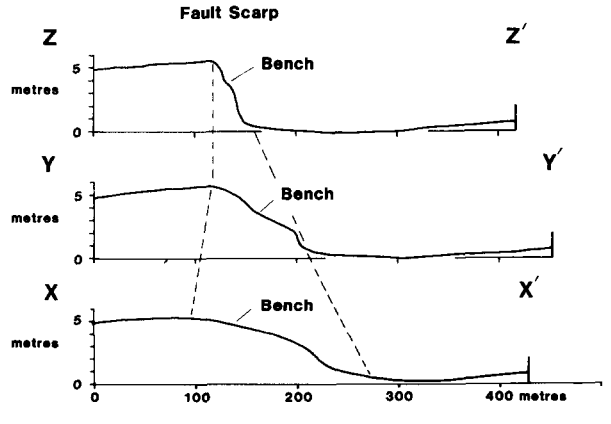

Fig. 11. Cross-sections across the Huangarua Fault scarp (located near D in Fig. 9) showing change from an abrupt scarp in the northeast, to a more distributed region in the southwest. Distinct bench may mark most recent rupture, which resulted in bifurcation of scarp.

The convergence point of strata in the zone of dip fanning (Figs. 6 and 7) of the Te Muna gravels can be considered as a hinge line separating that part of the fold that was uplifting relative to the drainage system (and therefore was being eroded) from that part which was subsiding and accumulating sediment. The gravels now lying above the unconformity surface indicate that the region of erosion eventually became an area of deposition, and hence the hinge line must have migrated NW. This could be due to either a local change in the fold geometry or a change in the overall drainage system. Folding must have begun after the deposition of the most steeply dipping strata within the zone of dip fanning. Comparison of this stratigraphic level with the type section defined by Collen and Vella (1984), indicates this to be about 1.0 ± 0.05 Ma, which gives a maximum age for the start of folding. The greater thickness of the Hautotara Formation on the steep limb of the Huangarua Syncline (100 m as opposed to 40 m elsewhere) suggests that this was an area of greater subsidence prior to 1.0 Ma, and with the commencement of folding it became an area of uplift. No folding appears to have taken place in the previous 9 Ma.

RATES OF DEFORMATION

The age and tilt of strata for different parts of the fold structures are shown in Table 1. Ages are taken from Collen & Vella (1984), Milne (1973) and Palmer (1982). Minimum average tilt rates (MATR), defined to be the present dip of the strata divided by its stratigraphic age (independent of strike of beds or plunge of folds) are between 10^{-4} and 10^{-6} degrees a^{-1} (Table 1). However, the tilt rate will vary with the position and time within a fold structure.

Average rates of shortening across the fold structures can be estimated from the cross-section in Fig. 4. This has been constructed assuming no thickening of the Te Muna Formation in the core of the Huangarua Syncline, while seismic reflection profiles suggest the synclinal trough may be 100–200 m deeper. Therefore the distance along the fold limb (R) between the crest of the Harris Ridge Anticline and trough of the Huangarua Syncline, normal to the fold axis is 1750 ± 100 m. The present horizontal separation is 1250 m, with a vertical separation of 1000 ± 100 m. Assuming that all folding started 1.0 Ma, this gives an average rate of horizontal shortening between the Harris Ridge Anticline crest and Huangarua Syncline trough, normal to the fold axis, of 0.5 ± 0.1 mm a^{-1}, and an average vertical rate of separation of 1.0 ± 0.1 mm a^{-1}.

The lack of internal deformation, and also the evidence that flexural-slip along discrete planes can account for a large proportion of the folding, suggest that simple models of incompressible deformation, preserving bed length, may be used to explain the variation of stratal tilt with time. These are explored below.

Model for incompressible deformation

It is assumed that folding is controlled by the bulk of the rock mass deposited prior to the folding, and that this maintains bedding thickness during folding. The cross-section of the Harris Ridge Anticline and Huangarua Syncline (Fig. 4) suggest that the competent limestones and consolidated sandstones (*ca* 300 m thick) within the Pukenui Limestone and older formations may have controlled the folding, forming a type of mechanical linkage which is not disrupted by faults and can be modelled as either an angular or concentric fold (Fig. 12). It is supposed that all strata deposited after the commencement of folding were rotated passively with the underlying rocks and did not affect the mechanics of the fold system. It is also assumed that the hinges of the folds did not migrate with respect to the folded strata with time (i.e. that there was no 'rolling' of the hinge lines).

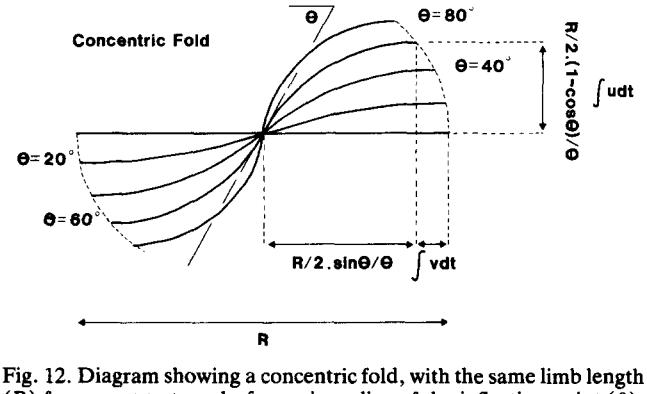

Fig. 12. Diagram showing a concentric fold, with the same limb length (R) from crest to trough, for various dips of the inflection point (θ). This models the evolution of the fold structure if it always remains an arc of a circle and the crest and trough do not migrate. Formulae relating the dip of the inflection point and limb length to the horizontal and vertical projections are also shown. u and v are the horizontal and vertical displacement rates relative to the inflection point.

If one fold limb of length R normal to the hinge line (i.e. from anticlinal crest to synclinal trough) is considered, the horizontal and vertical projections within any particular sedimentary horizon can be derived for both an angular and concentric fold (Fig. 12). Let θt = dip in radians of inflection point of fold limb at time t from the start of folding. The present tilt $\theta t'$ of strata of age t' is measured in the field. This can be normalized in terms of the evolution of the fold system such that:

$$t = T - t' \quad (1)$$

$$\theta t = \theta T - \theta t', \quad (2)$$

where T = age before present when folding started, and θT = present dip of strata that were horizontal at time T before present.

Angular fold

$$\text{Horizontal projection: } R \cos(\theta t) \quad (3)$$

$$\text{Vertical projection: } R \sin(\theta t). \quad (4)$$

Concentric fold

$$\text{Horizontal projection: } R(\sin(\theta t)/\theta t) \quad (5)$$

$$\text{Vertical projection: } R(1 - \cos(\theta t)/\theta t). \quad (6)$$

The horizontal and vertical projections (for unit limb length) normal to the fold axes (angular and concentric models) are plotted against time since the start of folding, using the data in Table 1 and equations (1)–(6). Tilt datum is assumed to represent that of the inflection point of the fold, neglecting the variation (±20°) in the strike of the beds. The gradient of the graph is v/R, where v is the rate of shortening or uplift between the fold trough and crest, and R is the fold limb length. Table 2 shows the various rates deduced from the plots, using a range of values for θT (present day dip of *ca* 1.0 Ma old strata).

Horizontal shortening in the Huangarua Syncline (Figs. 13 and 14)

The steep limb of the Huangarua Syncline (between the crest of the Harris Ridge Anticline and the trough of the Huangarua Syncline) is best modelled as part of a concentric fold. This model gives average rates of deformation for the last million years (horizontal rate 0.53 ± 0.15 mm a^{-1}; vertical rate 1.04 ± 0.15 mm a^{-1}) identical to those calculated from the cross-section. The angular model gives average rates which are too high. The concentric model suggests that the horizontal shortening rate increased considerably during the last 100 Ka from *ca* 0.53 mm a^{-1} to 0.88 ± 0.12 mm a^{-1} (Table 2, Fig. 13).

Data for the shallow limb of the Huangarua Syncline, modelled as part of an angular fold, also suggest a considerable increase in the shortening rate during the last 100 Ka (Table 2, Fig. 14). A further increase is indicated in the last 10 Ka. The combined rate across the steep and shallow limbs (a traverse of about 3250 m, including line ST in Fig. 3), averaged between 70 and

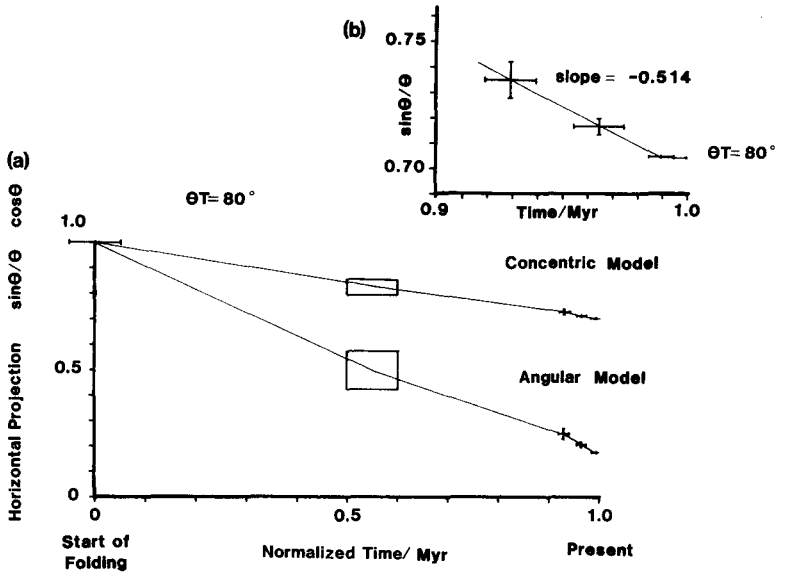

Fig. 13(a). Graph of normalized time against unit horizontal projection of fold from the crest of the Harris Ridge Anticline to the trough of the Huangarua Syncline. Both the concentric and angular fold models are used, with $\theta T = 80°$ (see text). Slope of line is proportional to the rate of shortening. Note the increase in the rate in the last 70 Ka. (b) Graph as in (a) enlarged for the last 70 Ka. Errors quoted in Table 2 encompass a range of θT. Note the zero rate in the last 10 Ka.

Table 2. Rates of horizontal and vertical movements for various parts of fold structures

Section	Type*	Width†	Model‡	Direction§	$R^{\|}$	$V_{cs}^{\P}$	θT^{**}	V_{av}††	V_1‡‡	V_2§§	$V_3^{\|\|}$
Harris Ridge Anticline crest to Huangarua Syncline trough	H	1250	C	160–150	1750 ± 100	0.5 ± 0.1	70–90	0.53 ± 0.15	0.53 ± 0.15	0.88 ± 0.12	0
Harris Ridge Anticline crest to Huangarua Syncline trough	H	1250	A	160–150	1000 ± 100	0.5 ± 0.1	70–90	0.85 ± 0.25	0.85 ± 0.2	1.3 ± 0.15	0
Harris Ridge Anticline crest to Huangarua Syncline trough	V		C		1750 ± 100	0.98 ± 0.1	70–90	1.04 ± 0.15		0.68 ± 0.17	0
Harris Ridge Anticline crest to Huangarua Syncline trough	V		A		1000 ± 100	0.98 ± 0.1	70–90	1.0 ± 0.15		0.5 ± 0.05	0
Shallow limb Huangarua Syncline (Line ST in Fig. 3)	H	~2000	A	150	2000		25	0.19	0.16	0.34	1.3 ± 1.0
Steep limb and shallow limb of Huangarua Syncline	H	3250	C + A	160–150				0.72 ± 0.15	0.69 ± 0.15	1.22 ± 0.12	1.3 ± 1.0
Line PR in Fig. 3	H	4450		150		0.76 ± 0.1					1.4 ± 0.4¶¶
Regions to southeast of study area	H	10,000	A	135			15–20	0.5 ± 0.15			0.95 ± 0.4¶¶

*Type of rate: horizontal (H) or vertical (V).
†Width across which rate is acting (in metres).
‡Fold model: concentric (C) or angular (A).
§Azimuth of traverse (in degrees).
‖ Length along fold limb applicable to model (m).
¶ Rate calculated from cross-section (in mm a^{-1}) = (length along fold limb − present separation)/age of folding.
** Dip (in degrees) of steepest strata controlling folding.
††Average rate since start of folding (1.0 Ma) (in mm a^{-1}).
‡‡Average rate between 1.0 Ma and 0.07 Ma (in mm a^{-1}).
§§Average rate between 0.07 Ma and 0.01 Ma (in mm a^{-1}).
‖‖ Average rate between 0.01 Ma and present day (in mm a^{-1}).
¶¶Calculated by multiplying by 1.6–2.1 (see text).

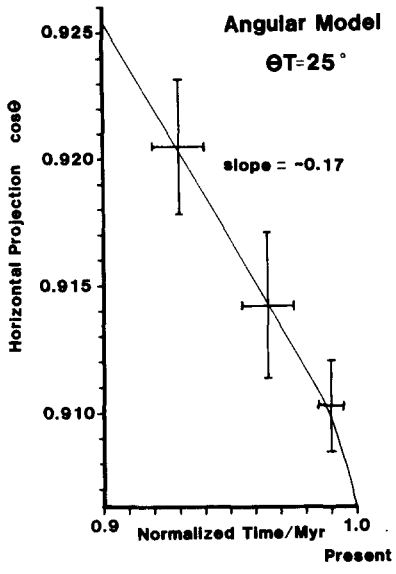

Fig. 14. Graph of normalized time against horizontal projection for shallow limb (angular model) of Huangarua Syncline (line ST in Fig. 4) for the last 70 Ka. Note the marked increase in rate (slope) in the last 10 Ka.

10 Ka, is 1.22 ± 0.12 mm a^{-1}, which is similar, although the uncertainty is large, to that for the last 10 Ka (1.3 ± 1.0 mm a^{-1}) when only the shallow limb has tilted. These rates are between 1.6 and 2.1 times the average rate over the last million years.

Shortening across larger areas

An estimate of the average horizontal rate of shortening across the whole study area can be made, assuming that there has been no length change parallel to the fold axes or strike-slip movement on the Huangarua Fault. The total shortening between points P and R in Figs. 3 and 4 has been calculated by adding as vectors the total shortening between P and Q, and Q and R. This gives an average rate between P and R (4450 m present day separation) for the last million years of 0.76 ± 0.1 mm a^{-1}. The increase in the rate during the last *ca* 100 Ka (1.6–2.1 times the average rate) observed in the Huangarua Syncline suggests that the rate of shortening between P and R will also have increased in this period to 1.4 ± 0.4 mm a^{-1}. If this rate is operating today, then the instantaneous strain rate is 3.1 ± 0.9 × 10^{-7} a^{-1} in a direction of 150°.

Vertical differential uplift (Fig. 15)

Plots comparing the vertical projection of the steep limb of the Huangarua Syncline and Harris Ridge Anticline with time do not fall on straight lines. The plots suggest an initial phase (up to about 400 Ka b.p.) of rapid differential uplift followed by a more reduced rate, though with an increase in the last 70 Ka. The concentric model suggests relative uplift rates of 0.68 ± 0.17 mm a^{-1} for the period 70–10 Ka, and zero for the last 10 Ka. The general decrease in the differential uplift rate, despite the increase in the rate of shortening in the last 100 Ka, is a consequence of the geometric constraints imposed on the fold model. As yet there is no independent evidence to determine whether the differential uplift rate has decelerated with time.

Relation of folding to faulting

No rotation of the steep limb of the Huangarua Syncline has occurred in the last 10 Ka, as young gravels show no tectonic tilt and the flexural-slip faults have been inactive. If the vertical differential movement

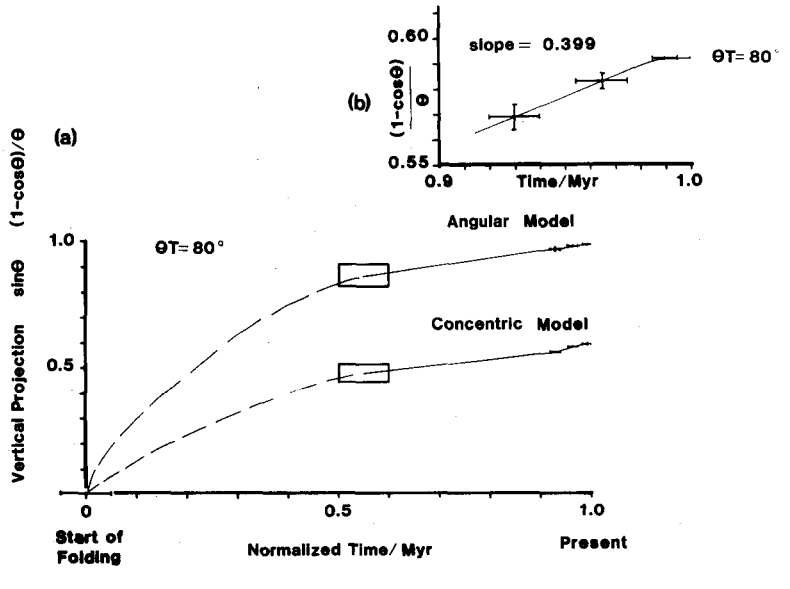

Fig. 15(a). Graph of normalized time against unit vertical projection between crest of the Harris Ridge Anticline and the trough of the Huangarua Syncline for concentric and angular fold models. Note the marked drop off in rate (slope) at about 0.6 normalized Ma (= 0.4 Ma b.p.), and slight increase again in last 70 Ka. Initial rate in both models is infinite which is clearly not realistic. (b) Graph as in (a) for the last 70 Ka. Note the zero rate during last 10 Ka, when Huangarua Fault was active.

between the crest of the Harris Ridge Anticline and trough of the Huangarua Syncline is expressed as a displacement on a fault instead of tilted strata, then the concentric fold model would predict a vertical fault displacement of 5.1–8.5 m in the last 10 Ka, using the uplift rates averaged between 70 and 10 Ka (0.68 ± 0.17 mm a^{-1}). These results compare well with a 5–6 m vertical offset of the *ca* 10 Ka Waiohine Gravel across the Huangarua Fault, assuming the fault is at least 10 Ka old. Part of the horizontal component of shortening on the steep limb of the Huangarua Syncline appears to have been taken up by an increase in the tilt rate on the shallow limb. This interplay between the accommodation of the strain by folding and faulting suggests that the Huangarua Fault, which appears to have moved intermittently (i.e. seismically), is a consequence of the folding. It is possible that the Huangarua Fault represents an accommodation structure required both by concentric folding (at depths greater than the radius of curvature) and the sinuous trace of the fold structure (discussed further on). The relation between the average vertical and horizontal rates of movement over the last million years (vertical > horizontal) between the crest of the Harris Ridge Anticline and trough of the Huangarua Syncline suggests that a fault at depth dips at *ca* 60°NNW. A fault beneath the Windy Peak Anticline would dip SE (Fig. 5). Although the asymmetric folds may have been initiated by fault movement at depth, once the folding started, the geometrical constraints (such as the preservation of stratal thickness, limb length and fold shape) may have mainly controlled fold development, as modelled here. In the later stages, especially when accommodation within the fold structure required internal faulting, the folding may have become more closely controlled by fault movement at depth.

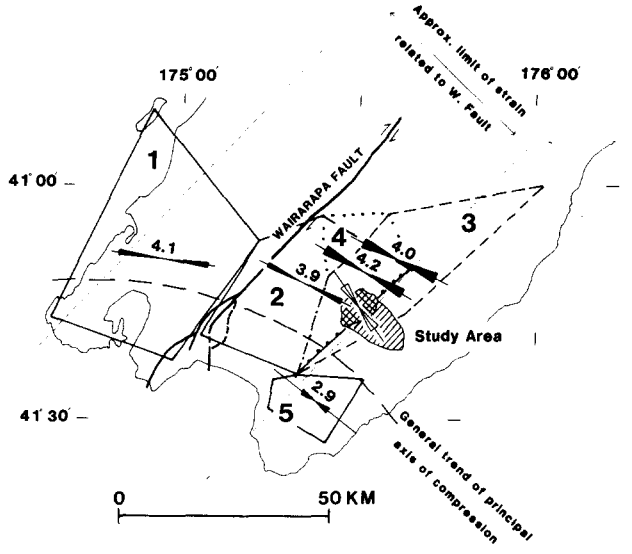

Fig. 16. Map of the southern part of the North Island showing networks used in retriangulation studies, orientation of principal axis of compression and the maximum shear strain rates for the various networks. The direction of shortening in the study area is also shown. The standard error in the orientation of the principal axis of compression is shown by the double fan shape, and the thin lines extending from each fan give an estimate of the standard error in the maximum shear strain rate (total length of bar is proportional to mean maximum shear strain rate plus one standard error). Heavy dashed line shows general trend in the orientation of the principal axis of compression across the plate-boundary zone. Light dashed lines parallel to the Wairarapa Fault show limit of area accumulating strain which could be released as a strike-slip displacement rate on the Wairarapa Fault.

LONG- AND SHORT-TERM DEFORMATION

Walcott (1978, 1984, personal communication) has deduced horizontal strain rates from retriangulation (geodetic) observations, mainly averaged over the last 50 years. Observations from networks covering the study area (Fig. 16, networks 2, 3, 4) are remarkably homogeneous within a 40 × 40 km grid, with a direction of maximum shortening orientated at *ca* 116° and with maximum shear strain rates of *ca* 4.0 × 10^{-7} a^{-1} (Fig. 16 and Table 3).

The retriangulation data can be expressed as two components $\dot{\gamma}_1$ and $\dot{\gamma}_2$, with reference to two orthogonal axes (x and y) orientated parallel and normal to the structural trend. $\dot{\gamma}_1$ equals $\partial u/\partial x - \partial v/\partial y$, and $\dot{\gamma}_2$ equals $\partial u/\partial y + \partial v/\partial x$, where u and v are the components of velocity of a point along the x and y axes, respectively. If one assumes that there is no velocity gradient along the length of the deforming zone (i.e. $[du, v/dx] = 0$), then $\dot{\gamma}_1$ is the instantaneous rate of shortening normal to the structural trend and $\dot{\gamma}_2$ is the instantaneous rate of simple shear parallel to the trend.

The swing seen in the direction of maximum shortening observed from the geodetic data (Fig. 16) indicates that the back part of the deforming prism is undergoing predominantly dextral shear ($\dot{\gamma}_2 > \dot{\gamma}_1$) parallel to the general structural trend, while the frontal parts are deforming predominantly by compression ($\dot{\gamma}_1 > \dot{\gamma}_2$) normal to the structural trend. This is shown by plots (Fig. 17) of the variation in the $\dot{\gamma}_1$ and $\dot{\gamma}_2$ components for a traverse across the emergent part of the prism (line

Table 3. Geodetic measurements for networks shown in Fig. 16

Network*	T†	$\dot{\gamma}_1$‡	$\dot{\gamma}_2$§	$\dot{\Gamma}$‖	ψ¶
1	53	0.12 ± 0.05	0.39 ± 0.03	0.41 ± 0.04	098 ± 3
2	53	0.31 ± 0.04	0.24 ± 0.04	0.39 ± 0.04	116 ± 3
3	41.5	0.31 ± 0.07	0.24 ± 0.06	0.40 ± 0.06	116 ± 7
4	52.5	0.36 ± 0.05	0.22 ± 0.05	0.42 ± 0.05	119 ± 6
5	87	0.28 ± 0.14	0.08 ± 0.13	0.29 ± 0.15	127 ± 11

*Network shown in Fig. 16.
†Time in years between triangulation surveys.
‡$\frac{\delta u}{\delta x} - \frac{\delta v}{\delta y}$ component of shear strain rate (10^{-6} rads a^{-1}) with standard error.
§$\frac{\delta u}{\delta y} + \frac{\delta v}{\delta x}$ component of shear strain rate (10^{-6} rads a^{-1}) with standard error.
x = positive to the southwest (225°), y positive to the southeast (135°).
u = component of velocity along x axis.
v = component of velocity along y axis.
‖Maximum shear strain rate (in 10^{-6} rads a^{-1}).
$\dot{\Gamma} = (\dot{\gamma}_1^2 + \dot{\gamma}_2^2)^{1/2}$.
¶Azimuth from true north of principal axis of compression with standard error, in degrees.

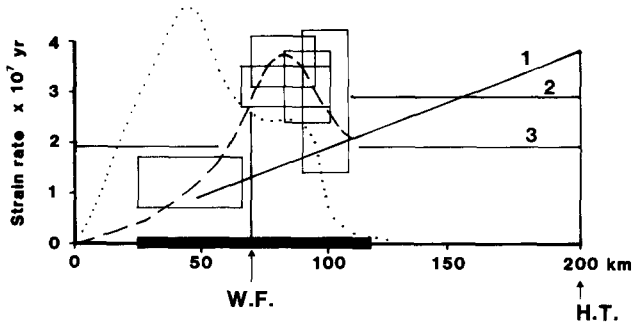

Fig. 17. Diagram showing the variation of the $\dot{\gamma}_1$ component (dashed line) and $\dot{\gamma}_2$ component (dotted line) of geodetic strain rate across the plate-boundary zone (parallel line AA′ in Fig. 1b) for axes parallel and normal to the general structural trend (045 and 135°, respectively). Note the marked separation of the two components: the $\dot{\gamma}_1$ component is greatest southeast of the Wairarapa Fault, while the $\dot{\gamma}_2$ component is greatest to the NW. Thickened part of distance axis represents the emergent part of the plate-boundary zone; W.F. = Wairarapa Fault, H.T. = Hikurangi trench. Boxes show range of values for one standard error about mean across whole width of network. Numbered lines are various hypothetical distributions of strain rate across plate-boundary zone resulting in a total convergence rate of 38 mm a^{-1}.

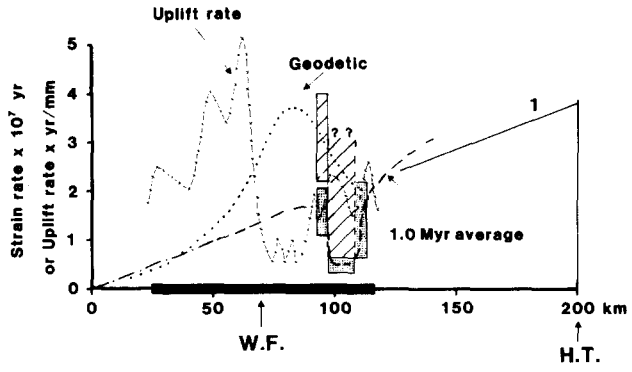

Fig. 18. Diagram illustrating geological strain rates determined from the study area and regions to the southeast. Obliquely shaded boxes represent geological strain rates averaged over the last 100 Ka, while dotted boxes are those averaged over the last 1 Ma. Dashed line is a smoothed pattern for the million year average; dotted line is the variation in the geodetic $\dot{\gamma}_1$ component (as in Fig. 17); alternating crosses and dashes show the pattern in uplift rates; solid line labelled (1) is a hypothetical distribution. Note negative correlation between uplift rates and geodetic rates.

AA′ in Fig. 1). Composite fault-plane solutions from seismicity (Kayal 1984) give an almost pure thrust sense of motion in the vicinity of the study area, with a slip vector trending *ca* 139°.

However, the orientation of the geological shortening direction in the study area does not compare well with the geodetic principal direction of compression. The geodetically observed strains are less than the elastic limit of rocks, and hence a large proportion of the $\dot{\gamma}_2$ component of geodetic strain in a wide area (>20 km) either side of the major strike-slip faults may be elastic strain which will ultimately be released as slip on these faults. Figure 16 shows the zone accumulating elastic strain, if an average slip rate of 12 mm a^{-1} (R. Grapes personal communication) on the Wairarapa Fault is expressed as a distributed shear strain rate of 2.4×10^{-7} a^{-1} (typical geodetic $\dot{\gamma}_2$ value). All of the geodetic networks are at least partly in this zone. Therefore probably only the compressional component of geodetic strain normal to the general structural trend ($\dot{\gamma}_1$ value) will result in permanent deformation in the vicinity of the study area, i.e. similar to the strain shown by the triangulation network furthest from the Wairarapa Fault (network 5 in Fig. 16).

A further complication exists as the structural trend in the study area is not always parallel to the regional trend. The difference is mainly due to the sinuous trace of the Huangarua Fault and Syncline. If the study area is only shortening normal to the regional structural trend (045°), a small dextral strike-slip motion (*ca* 0.6 mm a^{-1}) would be expected where the Huangarua Fault trends 160° (resulting in a 1:1 ratio between strike-slip and vertical movements), as well as a very small component of shortening along the axis of the Huangarua Syncline.

The shortening strain rates derived from geological structures ($3.1 \pm 0.9 \times 10^{-7}$ a^{-1}), assuming zero or 0.6 mm a^{-1} strike-slip motion on the Huangarua Fault averaged over the last 100 Ka, are entirely compatible with the geodetic $\dot{\gamma}_1$ component (Fig. 18). This suggests that the geodetic rates of shortening, even on such a limited time scale as 50 years are a good guide to the actual geological rates averaged over the last 100 Ka in the same area. Shortening strain rates based on rates averaged over the last million years are significantly less.

Regional long-term shortening

Gentle (15–20°) regional dips are maintained for about 10 km southeast of the study area. The dips steepen up to *ca* 35° even further to the southeast, where the deformed Mesozoic basement, on which the cover sequences rest unconformably, is exposed. The continuity of structure with the study area suggests that these dips have resulted from tectonic rotation in the last million years.

In these and other areas Ghani (1978) has defined growing anticlines and synclines, documented mainly from the heights of coastal wave-cut platforms, and a good correlation between topography and uplift rates. Ghani extrapolated the uplift pattern inland by calibrating the uplift of an inferred regional peneplain [summit height accordance, Wellman (1948)] with coastal and some inland data. This suggests that surfaces are uplifting at between 0.5 and 5 mm a^{-1} averaged over the last 100 to 200 Ka (Ghani, *op. cit.*), with wavelengths between 5 and 15 km and amplitudes expressed as an average differential uplift rate of *ca* 0.5–2.0 mm a^{-1} (Figs. 2 and 18). The whole study area has risen at least 1.5 mm a^{-1} averaged over the last 200 Ka. However the instantaneous strain rate suggested by the variation in uplift rates (tilting) using the angular fold model (0.4×10^{-7} a^{-1}) is considerably less than in the regions to the NW (Fig. 18). No evidence for large fault offsets (>100 m) is found, and major reverse faults, outcropping in adjacent areas, appear to die out along strike. Therefore movement at depth (possibly ramping) and back

rotation (*ca* 15° Ma^{-1}) of thrust sheets may be occurring in the gently-dipping areas, resulting in uplift and tilting on the limbs of the large wavelength anticlines. The base of such thrust sheets may not reach the surface until much further to the southeast, where a large amount of shortening could be accommodated. The study area may form part of such a thrust sheet or the tip of another overriding one.

Alternatively, small-scale surface faults may play an important role here in accommodating the surface shortening. Small fault offsets (<50 m) would remain undetected in these monotonous mudstone sequences. The geodetic strain rate requires shortening of 0.1–0.4 mm km^{-1} a^{-1}, while the uplift data suggest a differential uplift of *ca* 0.1 mm km^{-1} a^{-1}. These conditions can be satisfied by a variety of fault block models. However, this rate of shortening cannot have been maintained for more than *ca* 100 Ka as there is no evidence for the required fault displacements. The average rates of shortening in the gently dipping areas over the last million years must be close to those accommodated by tilting ($0.4–0.6 \times 10^{-7}$ a^{-1}, Fig. 18).

Crustal thickening and uplift

The horizontal strain rates normal to the structural trend should give an estimate of the rate of crustal thickening due to shortening, assuming no differential lateral transport of material parallel to the trend or addition from below. Taking a horizontal shortening strain rate of $3.1 \pm 0.9 \times 10^{-7}$ a^{-1} and a crustal thickness of 15 km resting on the subducted plate (Kayal 1984) as appropriate for the study area in the last 200 Ka, then this suggests that the average crustal thickening rate is 3.3–6.0 mm a^{-1} (shortening × crustal thickness). This is 1.9–3.4 times the average uplift rate of the land surface in the study area over the last 200 Ka (1.75 mm a^{-1}), indicating that if there is no surface erosion or addition of material from below, the area is being at most only half isostatically compensated. This is in agreement with an observed positive isostatic gravity anomaly which increases towards the southeast.

On a regional scale there is a negative correlation between the uplift rate and the geodetic and inferred geological shortening rates (Fig. 18). As there is no thermal anomaly, the uplift pattern must be a consequence of some combination of crustal shortening, degree of compensation, erosion rate and addition of material from below. The degree of isostatic compensation is likely to increase away from the trench, sympathetic with the decrease in the effects of the flexural rigidity of the subducted slab. The average erosion rates over the last 100 Ka are likely to be similar throughout the emergent prism, because all areas preserve relict land surfaces (Wellman 1948, Ghani 1978), and are certainly not high enough for the landscape to be in a steady state. Therefore the fast uplift rates must be controlled by addition of material from below. However the particularly fast uplift rates in the strike-slip zone would require the addition of enormous amounts of material (a thickness of 15 km brought in at the full plate convergence rate) if this area was being fully compensated. It is therefore likely that despite the large negative isostatic gravity anomaly in the back part of the prism, the crustal thickening rate is not more than two or three times the uplift rate. The strike-slip zone is therefore best modelled as a backtilting block, resting on a flexurally strong subducted slab, and overriding the internally deforming region to the southeast. In a similar fashion the areas to the southeast of the study area may form part of another backtilting block which is overriding regions even further southeast. This structural style will result in the most uplift in those areas which are undergoing the least internal deformation, and is likely to be a consequence of the large amount of relatively strong Mesozoic basement within the prism. The weak Upper Tertiary and Quaternary cover rocks form only a thin surface layer (<5 km thickness).

Geodetic, geological and plate tectonic strain rates

The relation between the geodetic, geological and average plate tectonic strain rates (both shear and shortening components) across the plate-boundary zone (line AA′ in Fig. 1) are illustrated in Figs. 17 and 18. If they all record the total plate convergence, then the areas under the curves should be the same (38 mm a^{-1} of shortening and 33 mm a^{-1} of strike-slip). Three hypothetical distributions of strain rate are shown in Fig. 17 to help comparison with the geological and geodetic rates. The slip rates on the major strike-slip faults during the last 10 Ka can account for at least 75% of the component of plate motion parallel to the general structural trend (Wellman 1972). The geological shortening strain rates, using rates averaged over the last million years and the present separations, suggest a strain rate distribution similar to line (1), with the highest strain rates occurring offshore, towards the subduction zone. However, it is clear that in detail the distribution of strain rates is more irregular with quite large fluctuations within the space of a few kilometres. During the last 100 Ka the rates are closer to the geodetic rates, suggesting that the normal convergence has been more widely distributed through the plate-boundary zone, with a distribution closer to hypothetical curve (2). However it is not clear whether the increase in rate in the last 100 Ka is unique, or whether similar fluctuations have occurred previously. Virtually no shortening appears to have occurred in the vicinity of the study area between 1 and 10 Ma, though it is very likely that subduction was continuous during this period. The simplest explanation is that deformation has progressively spread NW across the plate-boundary zone, reaching the study area in the last 1 Ma.

Seismic or aseismic deformation?

The evidence from the study area suggests that a large proportion, if not all, of the geodetically measured strain is redistributed during earthquakes. This is indicated by:

(i) the good agreement between the geological and geodetic strain rates, if it is assumed that the $\dot{\gamma}_2$ component represents elastic strain which will be released on major strike-slip faults; (ii) the interplay between the accommodation of strain by faulting and folding, and the lack of evidence for aseismic creep on any of the surface faults, but good evidence for discontinuous and hence probably seismic movement; (iii) the fold structures were probably initiated by faulting at depth, as they are markedly asymmetric, and they also pass along strike into major faults for which there is no evidence of continuous movement. This inferred lack of aseismic deformation is probably again a consequence of the large amount of old 'strong' Mesozoic basement in a region with a low geothermal gradient. Such areas are likely to behave differently from wide zones of continental deformation which are not underlain by a subducted slab and appear to deform predominantly aseismically (North 1974, 1977, Anderson 1985). In New Zealand one might therefore expect the behaviour of the crust in the plate-boundary zone to change further south in the Southern Alps, which is away from the effects of the subducted oceanic Pacific plate.

CONCLUSIONS

The observed geodetic strain rates in the southeastern part of the North Island show that the plate-boundary zone is accommodating in a distributed manner the entire relative motion of the plates, and the short-term deformation can be regarded as continuous. The strain rates derived from growing fold structures in the study area (geological strain rates) are best compared with the shortening component of the geodetic strain, normal to the structural trend. The shear component is likely to be occurring on strike-slip faults outside the study area. The geological strain rate, averaged over the last 100 Ka, are in good agreement with the geodetic shortening strain rate normal to the structural trend, suggesting that the deformation in the plate-boundary zone has been widely distributed during this period. However, geological strain rates averaged over 1 Ma are about half the 100 Ka average. This may reflect either a cyclicity in the distribution of deformation, or a unique increase. The geological strain rates also vary rapidly with position in the plate-boundary zone. The subducted plate appears to form a platform, stable with respect to vertical movements, upon which deformation in the overlying prism is occurring. The available evidence suggests that a large proportion of this deformation is occurring seismically. The style of deformation is probably a consequence of the predominance of strong Mesozoic crust in the plate-boundary zone.

Structures similar to those in the study area are observed in fossil plate-boundary zones, where they might be taken as evidence for deformation over a considerably longer period than required in the study area.

Acknowledgements—This paper has greatly benefited from the help of various people. Dick Walcott has been a tremendous source of advice and encouragement. John Collen provided help in the field, as well as making available his knowledge of the area. S. H. Lamb has a New Zealand University Grants Committee Fellowship.

REFERENCES

Anderson, H. 1985. Seismotectonics of the Western Mediterranean. Unpublished Ph.D. thesis, University of Cambridge, U.K.

Chase, C. G. 1978. Plate kinematics: the Americas, East Africa and the rest of the world. *Earth Planet. Sci. Lett.* **37**, 353–368.

Collen, J. D. & Vella, P. 1984. Hautotara, Te Muna and Ahiaruhe Formations, Middle to Late Pleistocene, Wairarapa, New Zealand. *J. R. Soc. N.Z.* **14**, 297–317.

Ghani, M. A. 1978. Late Cenozoic vertical crustal movements in the southern North Island, New Zealand. *N.Z. Jl Geol. Geophys.* **21**, 117–125.

Kayal, J. R. 1984. Microseismicity and tectonics at the Indian/Pacific plate boundary: southeast Wellington province, New Zealand. *Geophys. J. R. astr. Soc.* **77**, 567–592.

Kingma, J. T. 1967. Geological Map of New Zealand 1 : 250,000, Sheet 12, Wellington, 1st edn, Department of Scientific and Industrial Research, Wellington, New Zealand.

Milne, J. D. G. 1973. Upper Quaternary geology of the Rangitikei Drainage Basin, North Island, New Zealand. Unpublished Ph.D. thesis, Victoria University of Wellington, New Zealand.

North, R. G. 1974. Seismic slip rates in the Mediterranean and Middle East. *Nature, Lond.* **252**, 560–563.

North, R. G. 1977. Seismic moment, source dimensions, and stresses associated with earthquakes in the Mediterranean and Middle East. *Geophys. J. R. astr. Soc.* **48**, 137–161.

Palmer, A. 1982. The stratigraphy and selected properties of loess in Wairarapa, New Zealand. Unpublished Ph.D. thesis, Victoria University of Wellington, New Zealand.

Stern, T. A., Davey, F. J. & Smith, E. G. C. 1986. *Reflection Seismology: The Global Perspective* (edited by Barazangi, B. & Brown, L.). *Geodynamic Series* **13**, 121–132.

Vella, P. & Briggs, W. M. 1971. Lithostratigraphic names, Upper Miocene to Lower Pleistocene, Northern Aorangi Range, Wairarapa. *N.Z. Jl Geol. Geophys.* **14**, 253–274.

Walcott, R. I. 1978. Present tectonics and late Cenozoic evolution of New Zealand. *Geophys. J. R. astr. Soc.* **52**, 137–164.

Walcott, R. I. 1984. The kinematics of the plate boundary zone through New Zealand: a comparison of short- and long-term deformations. *Geophys. J. R. astr. Soc.* **79**, 613–633.

Wellman, H. W. 1948. Tararua Range Summit Height accordance. *N.Z. J. Sci. Technol.* **30**, 123–127.

Wellman, H. W. 1972. Rate of horizontal fault displacement in New Zealand. *Nature, Lond.* **237**, 275–277.